Remotely searching for *Noctiluca miliaris* in the Arabian Sea

P. Jeremy Werdell,[1,2,*] Collin S. Roesler,[3] and Joaquim I. Goes[4]

[1] NASA Goddard Space Flight Center, Greenbelt, Maryland, USA
[2] School of Marine Sciences, University of Maine, Orono, Maine, USA
[3] Department of Earch and Oceanographic Science, Bowdoin College, Brunswick, Maine, USA
[4] Lamont Doherty Earth Observatory, Columbia University, Palisades, New York, USA
* Corresponding author: jeremy.werdell@nasa.gov

INTRODUCTION

Reversing monsoonal winds in the Arabian Sea result in two seasons with elevated biological activity, namely the annual summer Southwest Monsoon (SWM; June to September) and winter Northeast Monsoon (NEM; November to March) [Wiggert et al., 2005]. Generally speaking, the SWM and NEM create two geographically distinct blooms [Banse and English, 2000; Levy et al., 2007]. In the summer, winds from the southwest drive offshore Ekman transport and coastal upwelling along the northwestern coast of Africa, which brings nutrient-rich water to the surface from below the permanent thermocline [Bauer et al., 1991]. In the winter, cooling of the northern Arabian Sea causes surface waters to sink, which generates convective mixing that injects nutrients throughout the upper mixed layer [Madhupratap et al., 1996]. This fertilization of otherwise nutrient-deplete surface waters produces one of the most substantial seasonal extremes of phytoplankton biomass and carbon flux anywhere in the world [Smith, 2005].

Patterns in phytoplankton bloom succession in the Arabian Sea have been observed to proceed as dominance by diatoms, then cyanobacteria, then dinoflagellates, with total abundances successively decreasing [Sawant and Madhupratap, 1996]. Small, autotrophic picoplankton (*Prochlorococcus* and *Synechococcus*) dominate the intermonsoon seasons, as these periods experience the lowest annual surface nutrient concentrations [Garrison et al., 2000]. The nitrogen-fixing cyanobacterium *Trichodesmium spp*. often also appears during these oligotrophic intermonsoon seasons when surface waters are nutrient depleted and low in total biomass. Large numbers (sometimes dense mats) of *Trichodesmium spp*. have been reported both along the (Indian and African) coasts and in the central areas of the Arabian Sea [Devassy et al., 1979].

Noctiluca miliaris (also known as *Noctiluca scintillans*) has emerged as an intermediate dominant species during the NEM [Chaghtai and Saifullah, 2006; Parab et al., 2006; Madhu et al., 2012]. *N. miliaris* is a large, green mixotroph that combines phytosynthesis from a chlorophyll containing endosymbiont (*Pedinomonas noctilucae*) with ingestion of prey [Elbrachter and Qui, 1998]. Gomes et al. [2014] speculated that *N. miliaris* maintains genetic predisposition to low oxygen conditions based on shipboard physiological studies. The authors correlated the emergence of *N. miliaris* in the northeast Arabian Sea in the 2000's with declines in oxygen saturation and phytoplankton diversity observed from the 1970's to 2000's. Other studies also reported observations of *N. miliaris* replacing *Trichodesmium spp*. in eastern Arabian Sea during intermonsoonal seasons [Parab et al., 2006]. The emerging predominance of *N. miliaris* is ultimately expected to alter predator-prey relationships of higher trophic levels and, thus, carbon export to the deep ocean [Smetacek and Cloern, 2008].

Here, we explore the use of ocean color satellite data records from the NASA Moderate Resolution Imaging Spectroradiometer onboard Aqua (MODISA) to discriminate between *N. miliaris* and diatoms, the dominant phytoplankton functional group observed to comprise blooms in the northern Arabian Sea during its annual NEM. Building upon Roesler et al. [2014] and Werdell et al. [2014], we proceeded with an ocean reflectance inversion algorithm (ORM; also referred to as a semi-analytical algorithm). The pigmentation of *P. noctilucae* produces sufficiently distinct greeen coloration that *N. miliaris* appears optically different from the red lineage taxa typically observed in the region (e.g., other dinoflagellates and diatoms). Following, the color of the water observed by the satellite instrument should reflect the phytoplankton community structure present in the upper euphotic zone. Werdell et al. [2014] proposed that the application and interpretation of an ORM can be successful in the Arabian Sea, but requires caution when interpreting the absolute magnitudes of the retrievals. In keeping with the results from the their forward simulations, we use this paper to present what can be learned from ocean color satellite data records to lay the foundation for future studies.

METHODS

The Ocean Reflectance Inversion Model

Werdell et al. [2013] presents the theoretical framework of our ORM (which we build upon the Generalized IOP (GIOP) framework) and Werdell et al. [2014] describes its application to the Arabian Sea. Briefly, satellite ocean color instruments measure the spectral radiance emanating from the top of the Earth's atmosphere at discrete visible and near-infrared wavelengths. Atmospheric correction algorithms are used to remove the contribution of the atmosphere from the total signal and produce estimates of remote sensing reflectances ($R_{rs}(\lambda)$; sr^{-1}), the light exiting the water normalized to the hypothetical conditions of a non-attenuating atmosphere with an overhead Sun [Gordon and Wang, 1994]. Bio-optical algorithms are applied to the $R_{rs}(\lambda)$ to produce estimates of geophysical quantities, such as the near surface concentration of the phytoplankton pigment chlorophyll a (C_{φ}; mg m^{-3}) [O'Reilly et al., 1998] and marine inherent optical properties (IOPs; IOCCG 2006]. Our ORM proceeds following the default configuration presented in Werdell et al. [2013], with the exception that it solves for four components: backscattering by particles ($b_{bp}(\lambda)$; m^{-1}), absorption by dissolved material and non-algal particles ($a_{dg}(\lambda)$; m^{-1}), absorption by diatoms ($a_{\varphi D}(\lambda)$; m^{-1}), and absorption by *N. miliaris* ($a_{\varphi N}(\lambda)$; m^{-1}). Recall that these four components can be expressed as the product of their mass-specific spectra (eigenvector; a^* or b^*) and magnitude (eigenvalue, M). Using $R_{rs}(\lambda)$ as input and *a priori* assigned eigenvectors, we estimate the eigenvalues using non-linear least-squares inversion.

Satellite data acquisition and processing

We acquired ~11,000 MODISA daily, spatially-extracted Level-2 files containing all or part of the Arabian Sea from the NASA Ocean Biology Processing Group (OBPG). These files represent a substantial time-series for MODISA, spanning January 2003 to December 2011, at ~1 km^2 spatial resolution at nadir. We applied the ORM to each MODISA image using the OBPG General Inherent Optical Property software framework (GIOP; [Werdell et al., 2013]) to generate estimates of M_{bp}, M_{dg}, $M_{\varphi D}$, and $M_{\varphi N}$ (and, thus, $b_{bp}(\lambda)$, $a_{dg}(\lambda)$, $a_{\varphi D}(\lambda)$, and $a_{\varphi N}(\lambda)$). We

also calculated C_φ using the OBPG standard algorithm (OC3M; [O'Reilly et al., 1998]). Satellite data processing and quality assurance followed Werdell et al. [2009]. Finally, we mapped each image to a 2 km equal area sinusoidal projection using OBPG software tools packaged as part of the SeaWiFS Data Analysis System (SeaDAS). For several analyses, we further binned these daily data into weekly or monthly composites following Campbell et al. [1995].

Supporting in situ *data*

Field experiments to study the transition from *N. miliaris* to diatoms in the northern Arabian Sea were conducted during the 2011 NEM onboard the Indian Fishery Oceanographic Research Vessel Sagar Sampada (Figure 1). Sampling dates ranged from 7-19 March 2011 and included diatom-dominant, *N. miliaris*-dominant, and mixed population stations (Table 1). Data collected at each station included water samples for analysis of pigments, absorption, and microscopy and vertical profiles of optical and hydrographic properties. Methods for the collection and processing of these data appear in Gomes et al. [2014], Roesler et al. [2014], and Thibodeau et al. [2014]. Of particular interest to this study are the fluorometric and microscopic analyses that quantify the presence or absence of *N. miliaris*, various diatoms, and other dinoflagellates at each sampling station. We adopted the results presented in Gomes et al. [2014] and Thibodeau et al. [2014] to identify the dominant species in the upper 20 m of each station and to catalog whether or not *N. miliaris* appeared anywhere via microscopic enumeration in this vertical span (Table 1). We did not expect the $R_{rs}(\lambda)$ observed by MODISA to include major contributions from phytoplankton community members residing deeper than 20 m [Werdell et al., 2014]. Ultimately, we only used these *in situ* observations to evaluate the utility of MODISA data products collected simultaneously during the field campaign.

RESULTS AND DISCUSSION

Application of the ORM to identify N. miliaris

In an ORM, the magnitudes of retrieved eigenvalues depend entirely on the magnitudes of the assigned eigenvectors. Therefore, the derived M_φ cannot universally represent concentrations unless the $a^*_\varphi(\lambda)$ are realistically scaled to mass-specific absorption spectra that represent in situ conditions at the time of observation (in which case, $M_\varphi = C_\varphi$) [Werdell et al., 2013]. We acknowledge that no single $a^*_\varphi(\lambda)$ can ubiquitously be applied to any water mass at all times. Nevertheless, Werdell et al. [2014] analyzed controlled, analytical simulations for the Arabian Sea and concluded that our ORM (as configured above) can effectively identify *N. miliaris* when it dominantly contributes to the shape and magnitude of $R_{rs}(\lambda)$. They recommended the use of $M_{\varphi D}$ and $M_{\varphi N}$ to determinate the binary presence or absence of *N. miliaris* and cautioned against trusting the absolute component $C_{\varphi D,N}$ or $a_{\varphi D,N}(\lambda)$ to infer anything definitively quantitative about species-specific total abundance or biomass.

We evaluated the ability of our ORM to discriminate between *N. miliaris* and diatoms by comparing coincident MODISA retrievals and in situ measurements (Figure 2). We ultimately adopted a thresholding system to indicate the presence of *N. miliaris* when $M_{\varphi D}$ and $M_{\varphi N}$ meet predefined conditions – a concept previously introduced by similar studies (e.g., [Subramaniam et al., 2002; Cannizzaro et al., 2008; Tomlinson et al., 2009]). To determine these conditions, we applied the ORM to the four clear daily images that MODISA captured of the northeastern

Arabian Sea from 7-19 March 2011 and extracted the viable $M_{\varphi D}$ and $M_{\varphi N}$ retrieved along the ship track of the 2011 field campaign. The sum of these two eigenvectors (= C_{φ}) largely tracked the in situ C_{φ}, with an average satellite-to-in situ ratio of 1.07. Using in situ measurements, Gomes et al. [2014] and Thibodeau et al. [2014] reported the dominant presence of *N. miliaris* at stations 1, 3 and 4 and a mild presence at stations 5–7 and 9–11 (Table 1). The eigenvalues from MODISA that correspond to *N. miliaris*-dominant stations suggest that $M_{\varphi D} \leq 0.3$ and $M_{\varphi N} \geq 1$ collectively indicate the unambiguous presence of *N. miliaris* (Figure 4). $M_{\varphi D}$ occasionally fell below zero for some stations to compensate for $a^*_{\varphi N}(\lambda)$ that imperfectly represented *N. miliaris* at the time. Our choice of 0.3 as a threshold for $M_{\varphi D}$ represents its average value for the transect.

For the stations not wholly dominated by *N. miliaris*, the ORM correctly identified combinations of *N. miliaris* and diatom populations in the upwelling zone along the coast of the Kathiawar Peninsula (stations 6 and 7) [Solanki et al., 2008], the site of the highest biomass observed in this study (Table 1). When the R/V Sagar Sampada transited west back to the patch of the then declining offshore bloom (between stations 7 and 8), the ORM again identified *N. miliaris*, which was observed in situ but not determined to be dominant within a transitioning population of diatoms to dinoflagellates (Table 1). The remaining shiptrack trajectory moved southeast into a dinoflagellate-dominated population, the region of lowest biomass in this study (Table 1). In concert with results from Werdell et al. [2014], the ORM retrieved mixed combinations of $M_{\varphi D}$ and $M_{\varphi N}$ in this region (stations 9–13), indicating phytoplankton populations not singly represented by either $a^*_{\varphi D}(\lambda)$ or $a^*_{\varphi N}(\lambda)$, but rather somewhere in between (which would be optically consistent with the presence of other dinoflagellates or a declining *N. miliaris* bloom).

To further verify the ORM, we examined a MODISA image collected during a known *N. miliaris* bloom (9 March 2011, Figure 3) and an image thought to be free of N. *miliaris* (21 October 2011, Figure 4). *N. miliaris* now appears routinely during the NEM, but has yet to be identified as dominant in the SWM or intermonsoon seasons [Gomes et al., 2008, 2014]. The March image corresponds to *in situ* station 3 (Figure 1, Table 1), while the October image simply provides a clear view of our study area after the SWM. In the March image, the ORM correctly identified the ν-shaped feature in the center of the image as dominated by *N. miliaris* (Figure 3B). Fortuitously, the R/V Sagar Sampada was stationed within this feature on this day. As for the transect presented in Figure 2, the ORM also identified *N. miliaris* in the upwelling zones of northwest India and along the coast of the Kathiawar Peninsula.

Two other structural features merit mentioning that relate to our subsequent interpretation of MODISA time-series. First, the ORM did not attribute the elevated C_{φ} concentrations in the northwest corner to *N. miliaris* (unfortunately, no *in situ* measurements exist to verify this). If true, this suggests that ORM identification of *N. miliaris* remains decoupled from C_{φ} abundance. Second, the offshore *N. miliaris* patterns were generally continuous – that is, not speckled throughout the image. This was also true for the October image, where false positives for *N. miliaris* only appeared sporadically along the cloudy northwest coast of India (Figure 4B). MODISA occasionally observes either elevated $R_{rs}(\lambda)$ along coastlines and at cloud edges because of adjacency effects (stray light into the field of view of the instrument) or depressed $R_{rs}(\lambda)$ because of cloud shadows. Either way, coastlines and cloud edges can alter the magnitudes of $\underline{R}_{rs}(\lambda)$, which ultimately controls the inverted M from the ORM. We ignored these effects since such instances of false positives were rare. As for verification of our approach, the ORM never substantially indicated the presence of *N. miliaris* in the October image, as desired. We

might expect dinoflagellate populations in this region, given the time of year and low(er) C_{φ}. In the October image, the ORM retrieved mixed $M_{\varphi D}$ and $M_{\varphi N}$ in the range of 0.05 to 0.2 (as in Figure 2), which has been shown to be indicative of dinoflagellates [Werdell et al., 2014].

N. miliaris *and the 2011 Northeast Monsoon*

MODISA imagery collected in mid-March 2011 demonstrates a process in the northern Arabian Sea that we are beginning to better understand (Figure 5) – namely, that *N. miliaris* now appears as a grazer on the fringes of diatom blooms. Temporal evaluation of ORM retrievals suggests the population progressed from diatoms to *N. miliaris* to dinoflagellates, with a corresponding reduction in total near-surface biomass. This was also observed onboard the R/V Sagar Sampada, which returned to the waning ν-shaped feature and observed dinoflagellates one week after first collecting *N. miliaris* [Thibodeau et al., 2014]. Diatoms (in the northwest and along the coast) and dinoflagellates (in the southeast) maintained the highest and lowest *in situ* C_{ϕ}, respectively (Table 1). Spatial evaluation of ORM retrievals shows *N. miliaris* appearing at the outside edges of several diatom populations. Consider the two white arrows presented in Figure 3D, both of which correspond with higher C_{ϕ} features. The upper feature maintains elevated $M_{\phi N}$ throughout and elevated $M_{\phi D}$ in its western half, which alludes to grazing of diatoms in the eastern half where the ORM indicated dominance by *N. miliaris*. The lower feature maintains a similar pattern, as if *N. miliaris* appeared but had not yet consumed the diatom population. Although the R/V Sagar Sampada did not visit these two features, diatoms were observed *in situ* near the ν-shaped feature from 7–10 March 2011, just not in dominance. Few diatoms remained when the ship returned to this region from 15–16 March 2011 [Thibodeau et al., 2014].

MODISA did not capture a clear view of our study area the week preceding our field campaign, which prohibited visual evaluation of the formation of the ν-shaped filament shown in Figures 3 and 5. However, we expect that the *N. miliaris* bloom observed during this field campaign on 9 March 2011 originated offshore of western India (perhaps grazing on diatoms that once fluorished in the upwelling region along the Kathiawar Peninsula or Pakistani coast) and, with time, stretched northwest towards southern Pakistan. This is consistent with previous *in situ* observations by Parab [Parab et al., 2006] and Gomes [Gomes et al., 2008]. The sequence of imagery in Figure 5 shows the recession of the ν-shaped *N. miliaris* feature by 11 March 2011 approximately 20 km to the west. An average advection rate of 0.1 m s^{-1} (~9 km day^{-1}) would have supported the movement of this feature. *N. miliaris* reemerged in the center of our imagery on 16 March 2011, perhaps due to entrainment of the edge of the dissipating-ν-shaped filament into the clockwise-flowing feature to the southeast (visible in the 11 March image). This would be consistent with our suggestion that background populations of *N. miliaris* sporadically bloom at the edges of other phytoplankton features. It remains tempting to suggest that these *N. miliaris* amassed to graze on the high biomass observed along the Kathiawar Peninsula on 11 March 2011. However, approximately 125 km separated the closest boundaries of these features, which would require two weeks to transit at the latter rate of advection. Following, the *N. miliaris* appearing along the Indian coastline from 9- 11 March 2011 are not the same as those appearing offshore on 16 March 2011. The reemergent features disappeared by 18 March 2011.

Composite imagery for the Northeast Monsoon

We generated 30 day composites of OC3M C_ϕ for February 15 through March 15 of each year from 2003 through 2011 (Figure 6). These values represent the mean of all C_ϕ values realized over the course of one month. The ephemeral filaments we sought previously have been eroded and do not naturally appear. That said, these monthly averages demonstrate annual differences in the total abundance and distribution of biomass on basin scales, which complements analyses conducted previously (e.g., [Banse and English, 2000; Goes et al., 2005]. As reported elsewhere, total C_ϕ typically follows a decreasing gradient from the northwest (Gulf of Oman) to southeast corners (southwest coast of India) of the imagery [Banse and English, 2000]. In general, our composited MODISA imagery does not suggest continuously increasing or decreasing C_ϕ abundance from 2003 to 2011. In fact, 2007 and 2008 appear to be the minimum and maximum over the first eight years shown. However, differences in sampling from year to year naturally bias our observations of total biomass. While each 2 km bin in these images was "seen" an average of ten times by MODISA, the true sample sizes varied from year to year. Several years realized varying patterns in pixels that failed entirely over the course of these 30 days. The Gulf of Oman, for example, routinely suffered from failures in MODISA retrievals, either through cloud coverage, proximity to land (e.g., adjacency effects such as stray light or atmospheric correction failure through poor aerosol model selection), or ORM inversion failure.

We sequentially evaluated every 2-km bin of every daily MODISA file in these time periods to spatially catalog the appearance of *N. miliaris* as determined by the ORM. As before, we used $M_{\phi D} \leq 0.3$ and $M_{\phi N} \geq 1$ to indicate its presence. Conducting this analysis on daily imagery (versus 30 day composites of $R_{rs}(\lambda)$) enabled capturing ephemeral structural features observed by MODISA. Figure 7 represents a two-dimensional frequency distribution of instances of identified *N. miliaris* for each 2-km bin. Spatially, these communities of *N. miliaris* varied unpredictably from year to year. However, their features remained fairly spatially contiguous, rather than randomly distributed and speckled. In concert with our previous observations and in accordance with previous studies (e.g., [Gomes et al., 2008]), the ORM identified *N. miliaris* in the offshore northern Arabian Sea in most years. Gomes et al. [2014], for example, reported counts of *N. miliaris* in 2009 that exceeded those from any previous year – and the ORM identified pixels as populated with *N. miliaris* inside their region of study (a similar transect to that conducted in 2011). The ORM identified *N. miliaris* in the northern Arabian Sea more (relatively) frequently than in the southwestern and central regions of the basin, as expected from the few available historical in situ data records. However, in situ observations of phytoplankton community structure in the southwestern and central Arabian Sea remain scarce, which makes quantitative assessment of ORM performance in these regions unverifiable. When identifying pixels as hosting *N. miliaris* in the southwestern and central Arabian Sea, either the ORM revealed *N. miliaris* features previously unseen – thereby introducing a different story than what can be told solely by discrete samples collected in the northern Arabian Sea – or, our regional tuning of thresholds to northern data confounded the ability of the ORM to produce meaningful values in these regions. Nevertheless, the spatial bins identified as hosting *N. miliaris* remained uncorrelated with the total C_ϕ observed over the same time period. In fact, the regions of highest biomass appear to be those known to be populated by diatoms [Gomes et al., 2008].

Our 30 day composited maps of C_ϕ (Figure 6) and *N. miliaris* identifications (Figure 7) from MODISA during the 2003–2011 NEMs provide qualitative rationale for the increased: (1) use of satellite data to study phytoplankton species succession, as ship-board *in situ* sampling alone

cannot capture desired temporal and spatial scales; (2) *in situ* sampling in alternate regions of the Arabian Sea to construct, verify, and evaluate bio-optical models that estimate phytoplankton species composition; (3) deployment of continuous *in situ* measurement systems (e.g., moorings and gliders) with capabilities for optically detecting *N. miliaris*, such as multichannel fluorescence [Thibodeau et al., 2014]; and, (4) coordination with complementary hydrographic modeling efforts, as knowledge of physical forcings on resident biology will enable improved interpretation of the satellite retrievals. Consider, for example, the temporal and spatial evolution of *N. miliaris* identified by MODISA in the boreal Winter of 2010–2011 (Figure 8). Shipboard and aircraft sampling alone could never have revealed the substantial presence of *N. miliaris* along the Iranian, Pakistani, and northwest Indian coastlines from December 2010 to mid-January 2011, nor how these features shifted to the southwest along the Kathiawar Peninsula in late January to mid-February 2011. In fact, at the time of our field campaign, the most significant populations of *N. miliaris* appear to have waned. Furthermore, the ORM identified *N. miliaris* features that C_ϕ alone did not indicate. Much like the imagery in Figures 6 and 7, the bins identified as containing *N. miliaris* did not correspond directly to those with highest C_ϕ abundance. Finally, the MODISA imagery suggested the possible presence of *N. miliaris* in regions that are typically undersampled in the field. Phytoplankton populations have not been routinely enumerated along the eastern coast of Africa or in the central part of the Arabian Sea. Assimilated data sets of oxygen distributions, however, indicate sufficiently declining concentrations (in the central Arabian Sea, at least) to reinforce our observations of *N. miliaris* emergence, given its predisposition for depleted oxygen conditions [Banse et al., 2013].

CONCLUDING REMARKS

We present a pragmatic approach for identifying *N. miliaris* in an otherwise mixed phytoplankton community using satellite ORM retrievals. Our approach avoids any inference of total standing stock of *N. miliaris* or diatoms (representing all other phytoplankton), but rather uses thresholds based on *in situ* measurements to infer simple presence or absence. We concede that many of our observations remain largely circumstantial. No irrefutable evidence emerged that unequivically points to N. milaris wholesale replacing diatoms during the NEM. The Arabian Sea challenges our ability to generate remote-sensing time-series that consistently provide glimpses of phytoplankton dynamics on temporal and spatial scales that accommodate seeing ephemeral features. And, high spatial resolution (<1 km) satellite data records that predate the first *in situ* observations of *N. miliaris* (pre mid-1990s) do not exist. That said, satellite imagery, such as that from MODISA, does provide substantial insight into phytoplankton dynamics that cannot be achieved by conventional *in situ* sampling alone and, furthermore, points to specific places and times for target validation activities. As demonstrated in Werdell et al. [2014], new satellite missions with improved spectral resolutions (such as the NASA Pre-Aerosols, Clouds, and ocean Ecosystems (PACE) instrument) should improve our collective abilities to identify phytoplankton community structure from space.

ACKNOWLEDGEMENTS

Many thanks to Mary Jane Perry, Andrew Thomas, Huijie Xue, Helga do Rosario Gomes, Prahbu Matondkar, Lee Karp Boss, Ivona Cetinic, Lachlan McKinna, and Chuck McClain for their ideas, advice, and comments in support of this work.

REFERENCES

Banse, K. and D.C. English (2000), Geographical differences in seasonality of CZCS- derived phytoplankton pigment in the Arabian Sea for 1978-1986, Deep Sea Res. II, 47, 1623–1677.

Banse, K., S.W.A. Naqvi, P.V. Narvekar, J.R. Postel, and D.A. Jayakumar (2013), Oxygen minimum zone of the open Arabian Sea: variability of oxygen and nitrate from daily to decadal time scales, Biogeosci. Disc., 10, 15455-15517.

Bauer, S., G.L. Hitchcock, and D.B. Olson (1991), Influence of monsoonally-forced Ekman dynamics upon surface layer depth and plankton biomass distribution in the Arabian Sea, Deep Sea Res., 38, 531–553.

Campbell, J.W., J.M. Blaisdell, and M. Darzi (1995), Level-3 SeaWiFS Data Products: Spatial and Temporal Binning Algorithms, S.B. Hooker, E.R. Firestone, and J.G. Acker, eds., NASA Tech. Memo. 104566, Vol. 32, NASA Goddard Space Flight Center, Green- belt, Maryland.

Cannizzaro, J.P., K.L. Carder, F.R. Chen, C.A. Heil, and G.A. Vargo (2008), A novel technique for detection of the toxic dinoflagellate, Karenia brevis, in the Gulf of Mexico from remotely sensed ocean color data, Cont. Shelf Res., 28, 137–158.

Chaghtai, F. and S.M. Saifullah (2006), On the occurence of green Noctiluca scintillans blooms in coastal waters of Pakistan, North Arabian Sea, Pak. J. Bot., 38, 893–898.

Devassy, V.P., P.M. Bhattathiri, P.M., and S.Z. Qasim, (1979), Succession of organisms following Trichodesmium phenomenon, Ind. J. Mar. Sci., 8, 89-93.

Elbrachter, M. and Y.Z. Qui (1998), Aspects of Noctiluca (Dinophyceae) population dynamics, in Physiological Ecology of Harmful Algal Blooms, M.D. Anderson, A.D. Cembella, and G.M. Hallegraeff, eds., NATO ASI G41, Springer, Berlin, pp 315–345.

Garrison, D.L., M.M. Gowing, M.P. Hughes, L. Campbell, D.A. Caron, M.R. Dennett, A. Shalapyonok, R.J. Olson, M.R. Landry, S.L. Brown, H-B. Liu, F. Azam, G.F. Steward, H.W. Ducklow, and D.C. Smith (2000), Microbial food web structure in the Arabian Sea: a US JGOFS study, Deep Sea Res. II, 47, 1386–1422.

Goes, J.I., P.G. Thoppil, H.R. Gomes, and J.T. Fasullo (2005), Warming of the Eurasian landmass is making the Arabian Sea more productive, Science, 308, 545-547.

Gomes, H.D.R., J.I. Goes, S.G.P. Matondkar, S.G. Parab, A.R.N. Al-Azri, and P.G. Thoppil (2008), Blooms of Noctiluca miliaris in the Arabian Sea - an in situ and satellite study, Deep Sea Res. I, 55, 751–765.

Gomes, H.D.R., J.I. Goes, S.G.P. Matondkar, E. Buskey, S. Basu, S. Parab, and P. Thoppil (2014), Massive outbreaks of Noctiluca scintillans blooms in the Arabian Sea due to spread

of hypoxia, Nature Comm., 5, doi:10.1038/ncomms5862/www.nature.com/naturecommunications.

Gordon, H.R. and M. Wang (1994), Retrieval of water-leaving radiance and aerosol optical thickness over the oceans with SeaWiFS: a preliminary algorithm, Appl. Opt., 33, 443– 452.

Gregg, W.W., W.E. Esaias, G.C. Feldman, R. Frouin, S.B. Hooker, C.R. McClain, and R.H.Woodward (2001), Coverage opportunities for global ocean color in a multimission era, IEEE Trans. Geo. Rem. Sens., 36, 1620–1627.

IOCCG (2006), Remote Sensing of Inherent Optical Properties: Fundamentals, Tests of Algorithms, and Applications, Z-P. Lee, ed., Reports of the International Ocean-Colour Coordinating Group No. 5, Dartmouth, Canada.

Levy, M., D. Shankar, J-M. Andre, S.S.C. Shenoi, F. Durand, and C.D.B. Montegut (2007), Basin-wide seasonal evolution of the Indian Ocean's phytoplankton blooms, J. Geophys. Res., 112, doi:10.1029/2007JC004090.

Madhu, N.V., R. Jyothibabu, P.A. Maheswaran, K.A. Jayaraj, and C.T. Achuthankutty (2012), Enhanced chlorophyll a and primary production in the northern Arabian Sea during the spring intermonsoon due to green Noctiluca scintillans bloom, Mar. Bio. Res., 8, 182–188.

Madhupratap, M., S.P. Kumar, P.M.A. Bhattathiri, M.D. Kumar, S. Raghukumar, K.K.C. Nair, and N. Ramaiah (1996), Mechanism of the biological response to winter cooling in the northeastern Arabian Sea, Nature, 384, 549–552.

O'Reilly, J.E., S. Maritorena, B.G. Mitchell, D.A. Siegel, K.L. Carder, S.A. Garver, M. Kahru, and C.R. McClain (1998), Ocean color chlorophyll algorithms for SeaWiFS, J. Geophys. Res., 103, 24937–24953.

Parab, S.G., S.G, Prabhu Matondkar, H.D.R. Gomes, and J.I. Goes (2006), Monsoon driven changes in phytoplankton populations in the eastern Arabian Sea as revealed by microscopy and HPLC pigment analysis, Cont. Shelf Res., 26, 2538–2558.

Roesler, C.S., P.J. Werdell, H.D.R. Gomes, J.I. Goes, and S.G.P. Matondkar (2014), Remote detection of Noctiluca miliaris in the Arabian Sea, in review at Rem. Sens. Environ..

Sawant, S. and M. Madhupratap (1996), Seasonality and composition of phytoplankton in the Arabian Sea, Cur. Sci., 71, 869–873.

Smetacek, V. and J.E. Cloern (2008), On phytoplankton trends, Science, 319, 1346–1348.

Smith, S.L. (2005), The Arabian Sea of the 1990s: New biogeochemical understanding, Prog. Oceaogr., 65, 113–115.

Solanki, H.U., P.C. Mankodi, R.M. Dwivedi, and S.R. Nayak (2008), Satellite observations of main oceanographic processes to identify ecological associations in the Northern Arabian Sea for fishery resources exploration, Hydrobio., 612, 269–279.

Subramaniam, A., C.W. Brown, R.R. Hood, E.J. Carpenter, and D.G. Capone (2002), Detecting Trichodesmium blooms in SeaWiFS imagery, Deep Sea Res. II, 49, 107–121.

Thibodeau, P.S., C.S. Roesler, S. Drapeau, P. Matondkar, J.I. Goes, and P.J. Werdell (2014), Locating Noctiluca miliaris in the Arabian Sea: an evaluation of in situ multispectral fluorescent signatures, in press at Limnol. Oceanogr..

Tomlinson, M.C., T.T. Wynne, and R.P. Stumpf (2009), An evaluation of remote sensing techniques for enhanced detection of the toxic dinoflagellate, Karenia brevis, Rem. Sens. Environ., 113, 598–609.

Werdell, P.J., S.W. Bailey, B.A. Franz, L.W. Harding Jr., G.C. Feldman, and C.R. McClain (2009), Regional and seasonal variability of chlorophyll-a in Chesapeake Bay as observed by SeaWiFS and MODIS-Aqua, Rem. Sens. Environ., 113, 1319-1330.

Werdell, P.J., B.A. Franz, S.W. Bailey, and 16 co-authors (2013), A generalized ocean color inversion moodel for retrieving marine inherent optical properties, Appl. Opt., 52, 2019–2037.

Werdell, P.J., C.S. Roesler, and J.I. Goes (2014), Discrimination of phytoplankton functional groups using an ocean reflectance inversion model, Appl. Opt., 53, 4833–4843.

Wiggert, J.D., R.R. Hood, K. Banse, and J.C. Kindle (2005), Monsoon-driven biogeochemical processes in the Arabian Sea, Prog. Oceanogr., 65, 176–213.

TABLES

	Date	Latitude	Longitude	Chlorophyll *a* Concentration	Dominant Group	*N. miliaris* Identified
1	Mar 7	21.750	66.771	1.01±0.20	*N. miliaris*	Yes
2	Mar 8	21.361	66.806	0.35±0.02	Dinoflagellates	No
3	Mar 9	21.922	67.008	1.13±0.26	*N. miliaris*	Yes
4	Mar 10	21.984	67.018	0.74±0.01	*N. miliaris*	Yes
5	Mar 11	21.987	67.977	0.83±0.07	Diatoms	Yes
6	Mar 12	21.917	69.096	2.49±0.04	Diatoms	Yes
7	Mar 13	20.995	70.007	3.52±0.15	Diatoms	Yes
8	Mar 14	21.306	67.744	0.24±0.02	Dinoflagellates	No
9	Mar 15	21.378	66.786	0.30±0.06	Dinoflagellates	Yes
10	Mar 16	21.132	66.902	0.19±0.01	Dinoflagellates	Yes
11	Mar 17	19.987	67.984	0.21±0.01	Dinoflagellates	Yes
12	Mar 18	17.988	68.058	0.13±0.01	Dinoflagellates	No
13	Mar 19	18.004	70.045	0.22±0.01	Dinoflagellates	No

Table 1. Phytoplankton properties of the upper 20 meters of *in situ* stations visited in 2011. We present the concentration of chlorophyll *a* (mg m^{-3}) as the mean +/- standard deviation of duplicate or triplicate samples analyzed by high performance liquid chromotography. We determined the "dominant group" based on the vertical fluorometric analyses presented in Thibodeau et al. [2014]. Gomes et al. [2014] provided the microscopic cell counts to verify whether or not *N. miliaris* was identified at each station. Temparature and salinity ranged from 23.5 to 24.25^{o}C and 35.5 to 36.25 g kg^{-1}, respectively. Thibodeau et al. [2014] concluded that the observed *N. miliaris* could not be associated with these hydrographic characteristics.

FIGURES

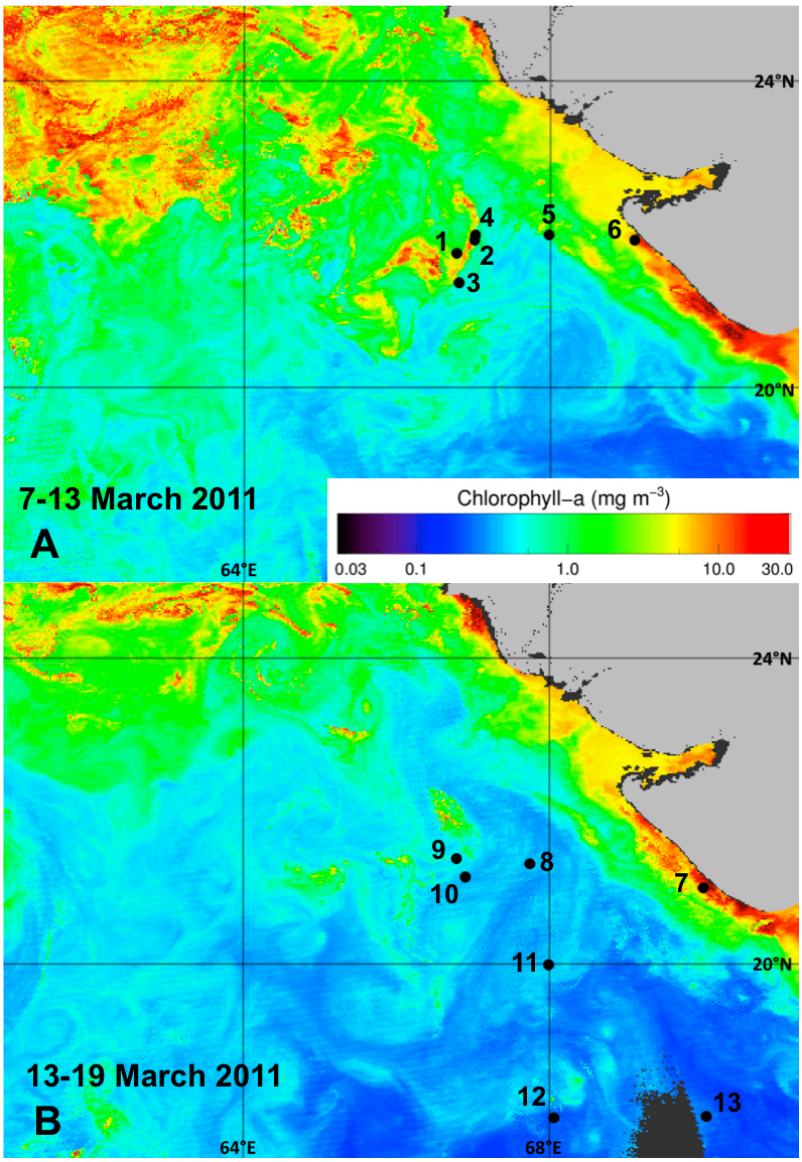

Figure 1. MODISA weekly C_φ (OC3M) composites collected during the 2011 field campaign at 2 km spatial resolution. Regions of grey and black indicate land and no satellite retrievals, respectively. Solid black circles show in situ sampling stations. We show two temporal ranges: (A) 7-13 March 2011, encompassing stations 1 to 6; and, (B) 13-19 March 2011, encompassing stations 7 to 13.

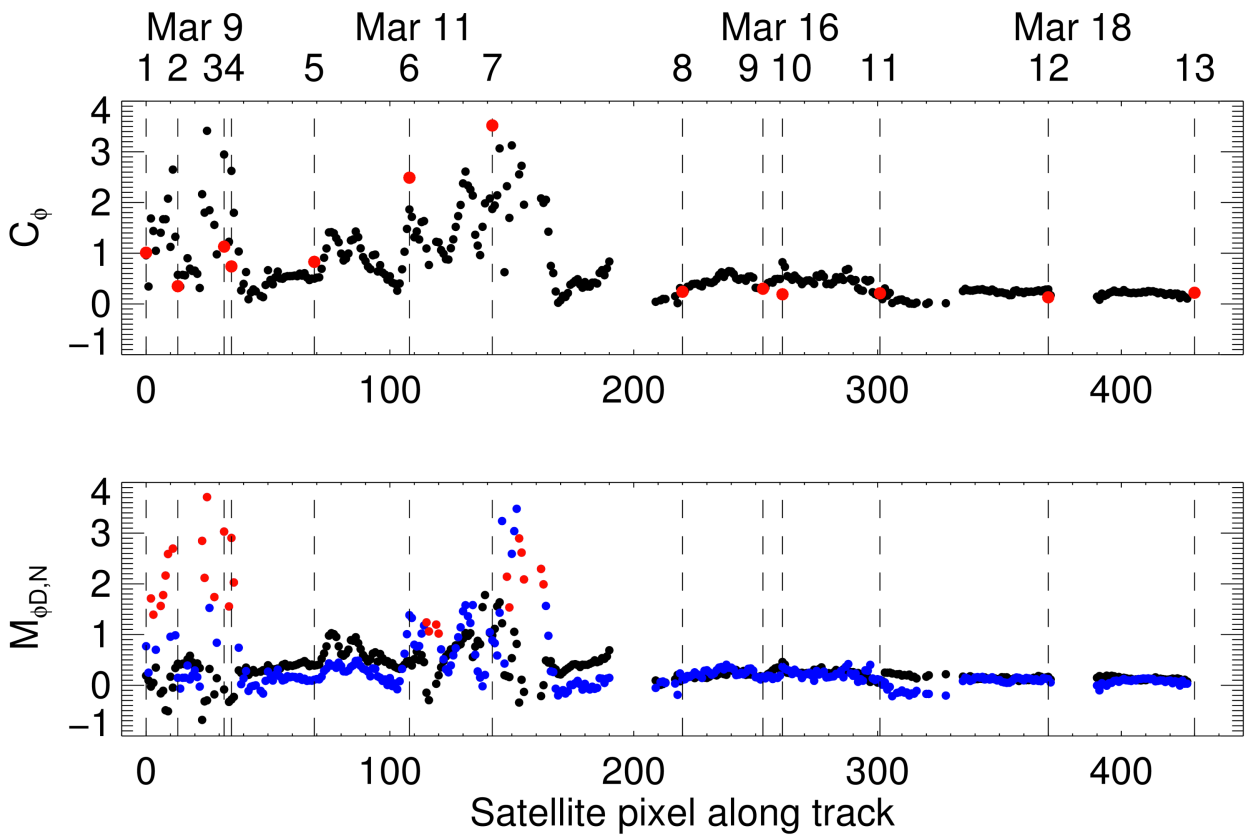

Figure 2. C_φ (top panel) and *N. miliaris* and diatom eigenvalues ($M_{\varphi N}$ and $M_{\varphi D}$; bottom panel)) from 2 km MODISA imagery along the cruise track of the 2011 field campaign. We applied the ORM to the four clear images that MODISA acquired during our field campaign (Mar 9, 11, 16 and 18). Vertical dashed lines indicate the in situ sampling stations. In the top panel, solid black circles show MODISA C_φ (= $M_{\varphi D}$ + $M_{\varphi N}$ from GIOP) and solid red circles show *in situ* C_φ (see also Table 1). In the bottom panel, solid black circles show $M_{\varphi D}$ and solid red and blue circles show $M_{\varphi N}$. The red circles indicate where $M_{\varphi D} \leq 0.3$ and $M_{\varphi N} \geq 1$.

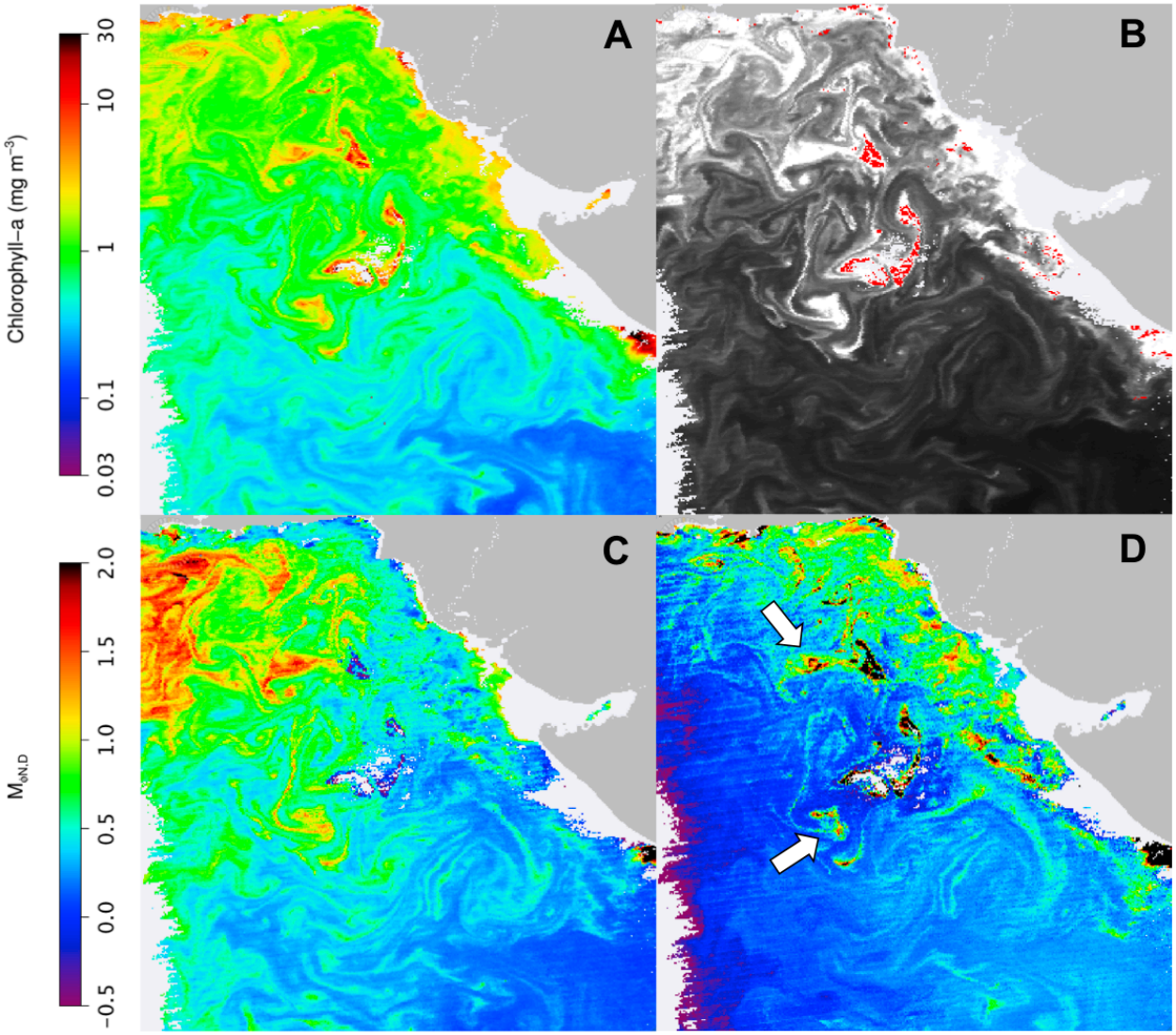

Figure 3. MODISA imagery of 9 March 2011, spatially mapped to 2 km. Regions of grey and white indicate land and no satellite retrievals, respectively. Panel (A) shows C_φ (OC3M). Panel (B) shows C_φ (OC3M) in greyscale, with red showing pixels where the ORM detected *N. miliaris* using thresholds of $M_{\varphi D} \leq 0.3$ and $M_{\varphi N} \geq 1$. Panels (C) and (D) show $M_{\varphi D}$ and $M_{\varphi N}$, respectively.

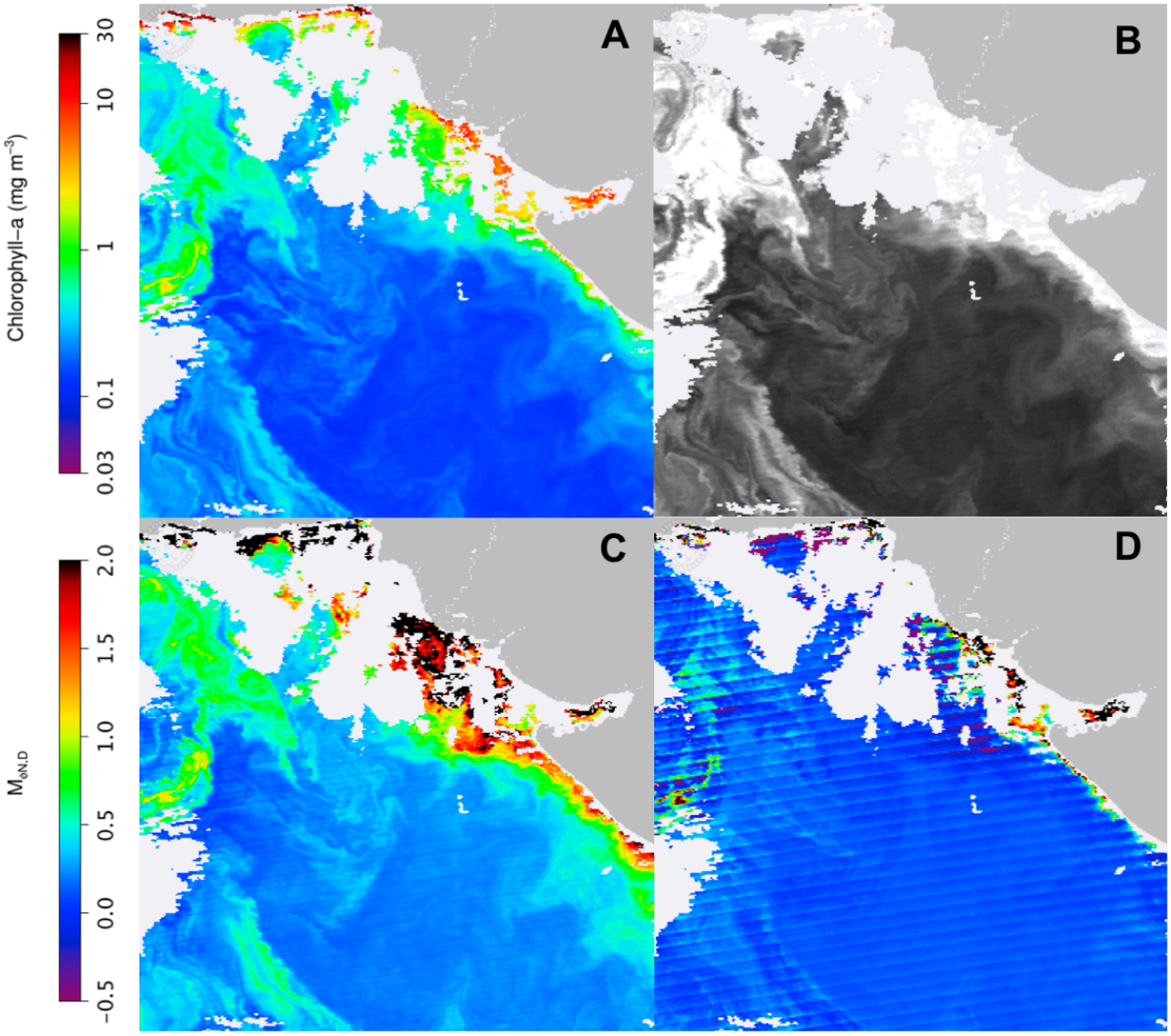

Figure 4. As in Figure 5, but for 21 October 2011.

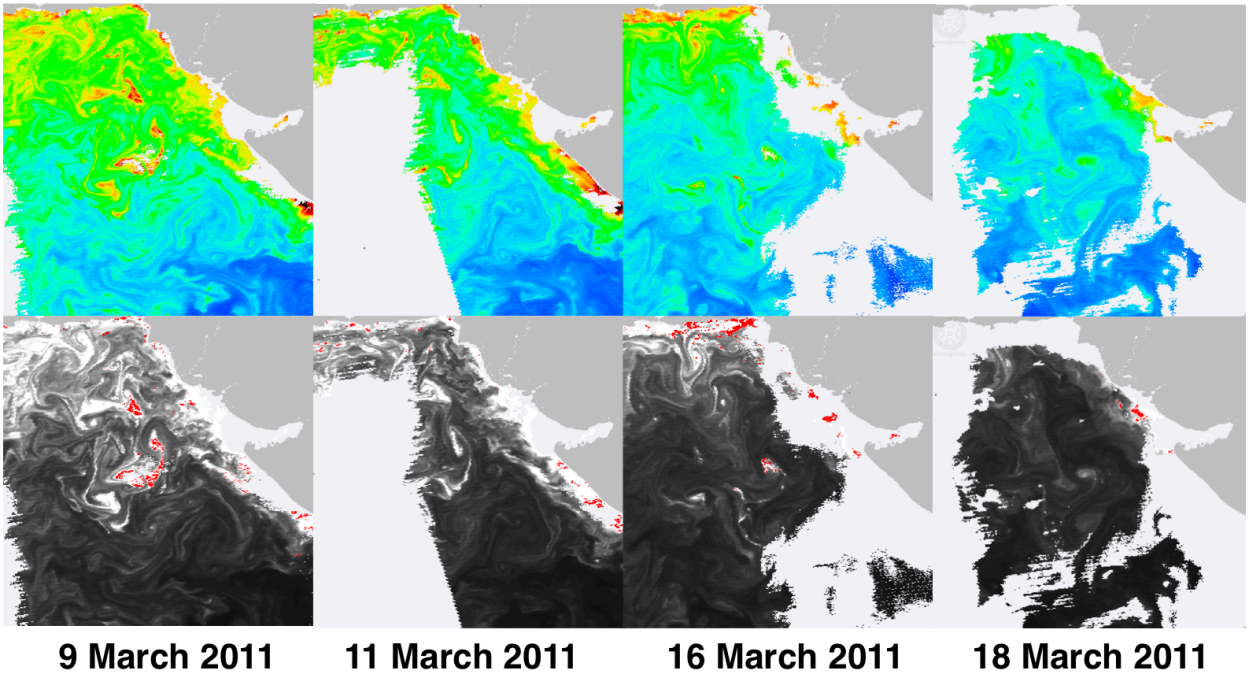

Figure 5. Four days of MODISA C_φ (OC3M) imagery during the 2011 NEM. Top row shows C_φ for each day. Bottom row shows C_φ in greyscale, with red showing pixels where the ORM detected *N. miliaris* using thresholds of $M_{\varphi D} \leq 0.3$ and $M_{\varphi N} \geq 1$. These images represent the only expansive, clear views of our study area that MODISA collected during this time period. Colorbar as in Figures 3 and 4. Regions of grey and white indicate land and no satellite retrievals (including ORM failure), respectively.

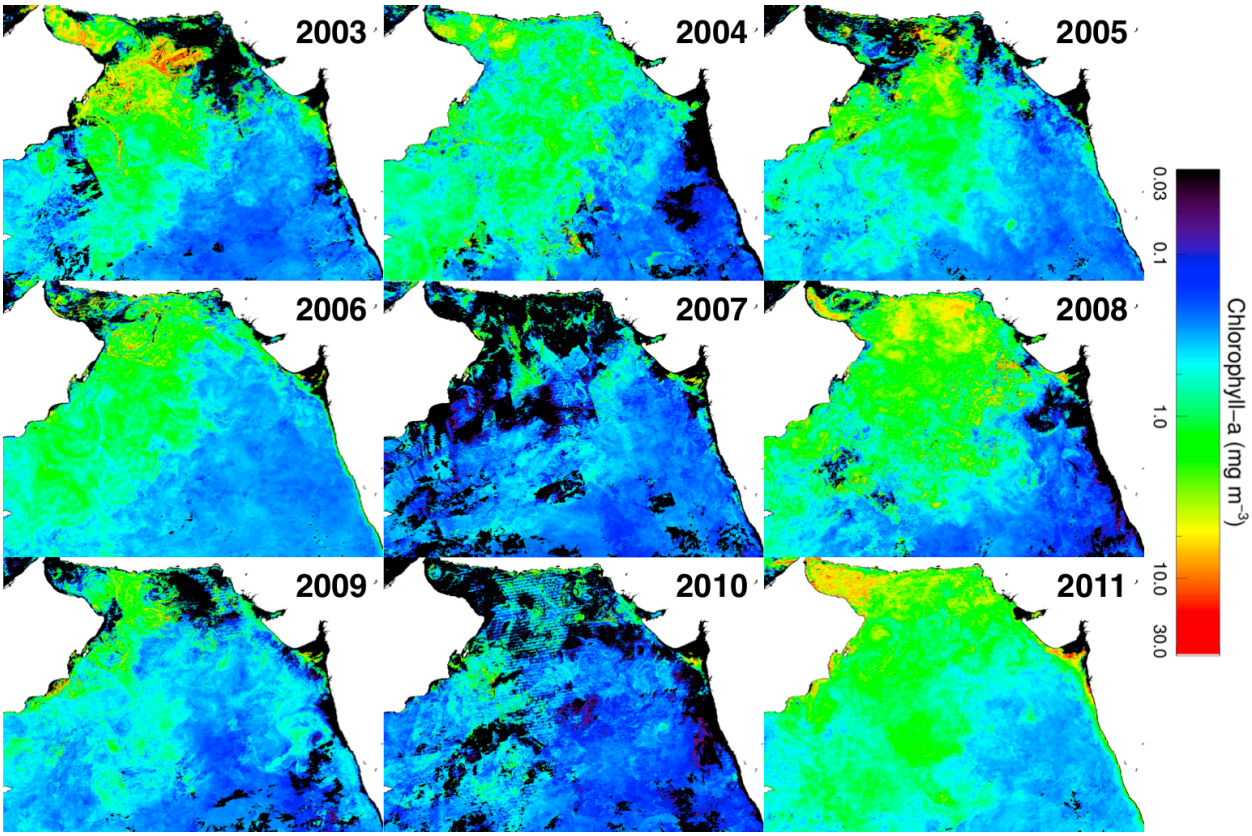

Figure 6. Annual four week composites of MODISA C_φ (OC3M) at 2 km spatial resolution. The four weeks encompass February 15 through March 15. Regions of white and black indicate land and no satellite retrievals (including ORM failure), respectively.

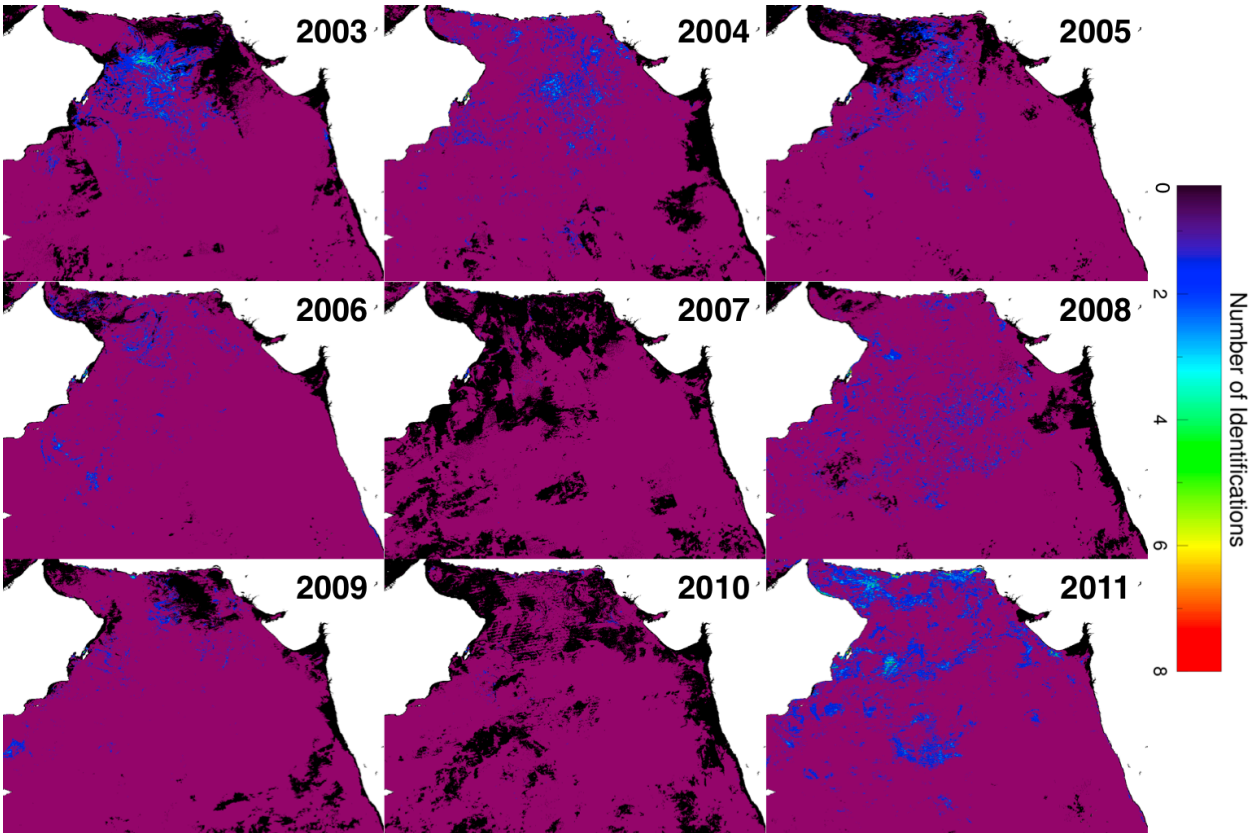

Figure 7. Annual four week geographic distributions of *N. miliaris* at 2 km spatial resolution as identified by our ORM using thresholds of $M_{\varphi D} \leq 0.3$ and $M_{\varphi N} \geq 1$. The four weeks encompass February 15 through March 15. Regions of white and black indicate land and no satellite retrievals (including ORM failure), respectively. Other colors show the number of times the ORM identified *N. miliaris* in a given 2 km bin. Purple indicates zero identifications. MODISA observed a given bin approximately 10 times each year on average.

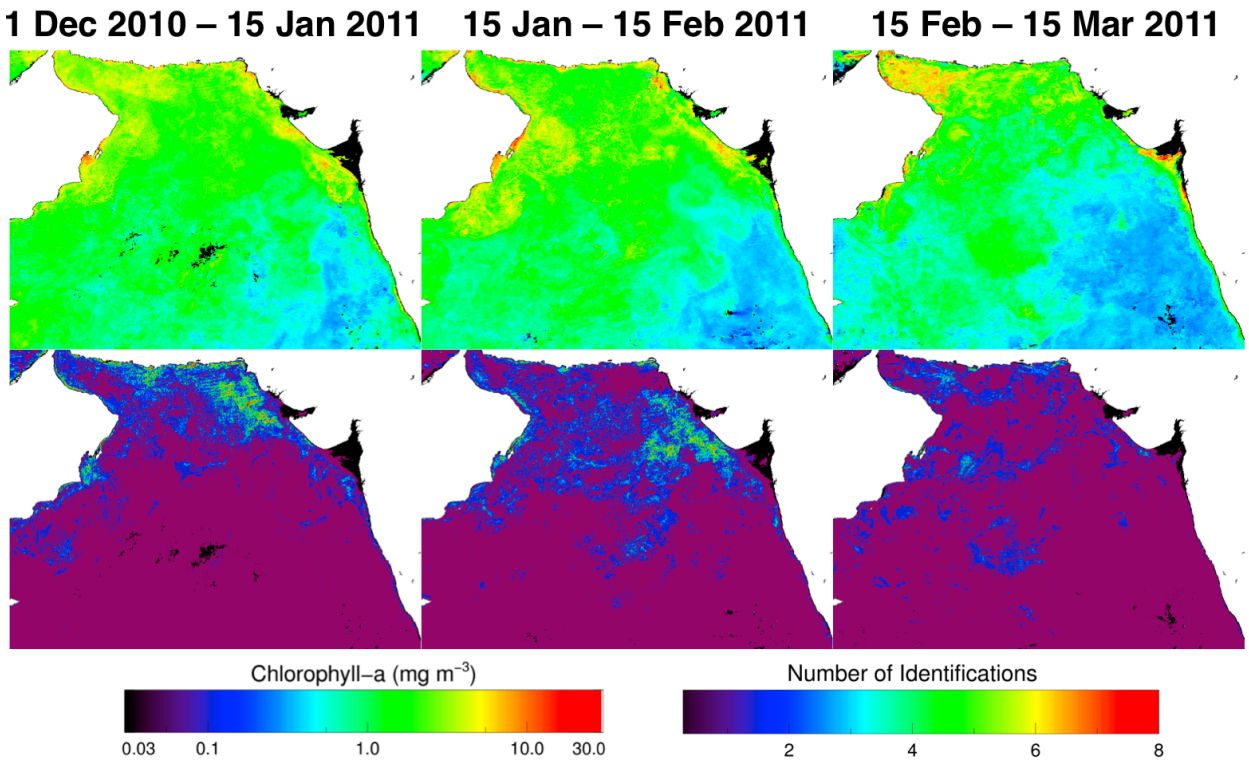

Figure 8. Progression of the geographic distribution of *N. miliaris* during the boreal Winter of 2010-2011 at 2 km resolution. Top row shows MODISA C_{φ} (OC3M) as in Figure 6. Bottom row shows *N. miliaris* identified as in Figure 7. Regions of white and black indicate land and no satellite retrievals (including ORM failure). Three sequential time periods are shown from left to right: 1 Dec 2010 to 15 Jan 2011, 15 Jan to 15 Feb 2011, and 15 Feb to 15 Mar 2011.